Supporting Information

S1. Literature data review

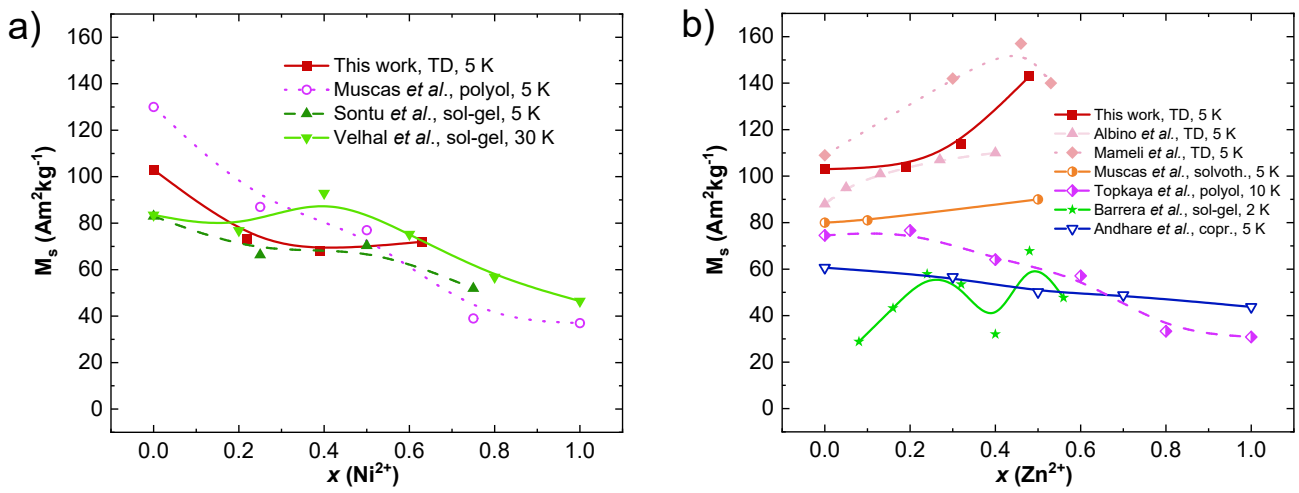

Figure S 1. Low-temperature saturation magnetization of a) Ni-Co[1–3] *and b) Zn-Co*[4–9] *ferrites from literature.*

S2. X-Ray Diffraction (XRPD)

Structural information about the samples was obtained by means of X-Ray powder diffraction techniques (XRPD), which are based on the diffraction phenomena arising from the interaction between X-Rays and a crystal lattice. A diffraction signal is obtained whenever, at a certain angle θ, the path difference among incident photons is an integer multiple of the X-Ray wavelength λ. These conditions are expressed by the Bragg law:

$$n\lambda_{Cu} = 2d_{hkl}\sin\theta \qquad \text{(S1)}$$

where d_{hkl} is the distance between two crystal planes. XRPD patterns were acquired with a Bruker D8 Advance diffractometer (solid state LynxEye detector, Cu Kα radiation, Bragg Brentano geometry, DIFFRACT plus software). In the hypothesis of spherical-shaped crystallites, the Scherrer equation can be used to estimate the average crystal size, based on the position and the full width at half of the maximum value of a certain peak:

$$\langle d_{XRD}\rangle = \frac{K\lambda_{Cu}}{F\cdot\cos\theta_c} \qquad \text{(S2)}$$

where $\langle d_{XRD} \rangle$ is the average size of the crystals, K is a constant depending on shape and size distribution of NPs, which is assumed to be 0.9[10], λ_{Cu} is the average wavelength of K_α and K_β radiation of Cu ($\lambda = 0.154187\ nm$)[11], θ_c is the Bragg angle on which the peak in centered in radians, and F is the *full width half maximum* of the selected peak. Three peaks – *i.e.,* (220), (311) and (400) – were fitted with a Pseudo-Voigt function to obtain θ_c and F.

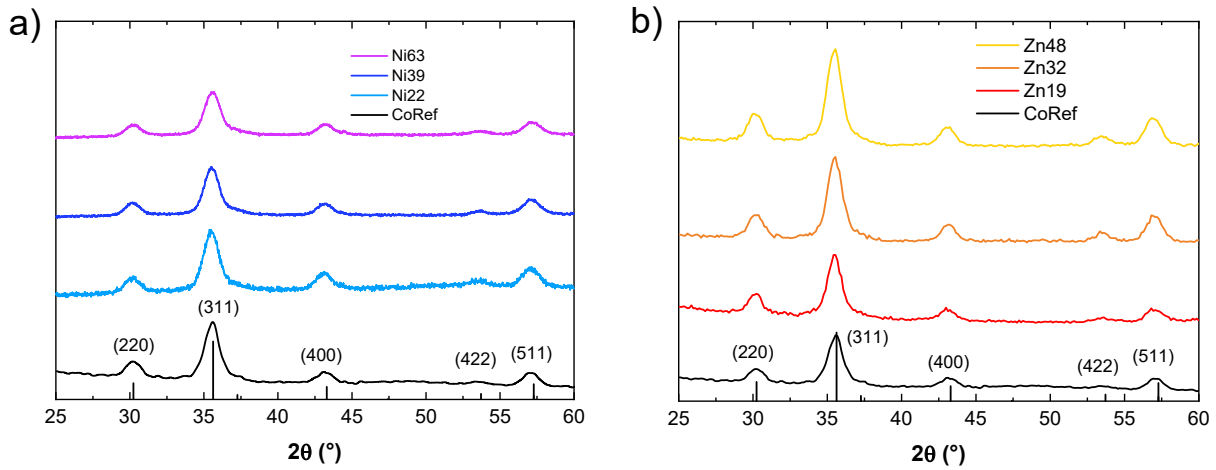

Figure S 2. XRPD patterns for a) the Ni-series and b) the Zn-series.

S3. Transmission electron microscopy morphological characterization

TEM images are elaborated to obtain a statistical overview of particle's dimensions and shapes, which have an influence on the magnetic properties of a nanostructured material. All the TEM images were elaborated with ImageJ software, which is able to recognize, measure and count black objects onto a white background. All the images as obtained images consist in blurred shapes and grey shades, thus image elaboration is necessary. Fig. S2 illustrates the main steps off the elaboration, which briefly consist in adjusting brightness and contrast of the image in order to make nanoparticles' border sharper and easily recognizable. Then the picture is turned into a black and white binary version which can be automatically measured by the software. The particles clusters which are not separated in the final image are removed at the end of the elaboration.

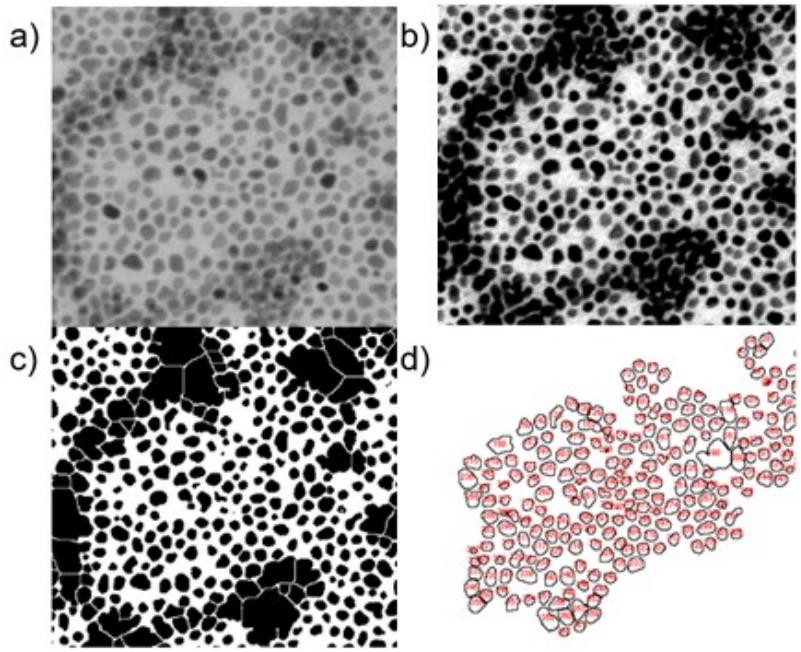

Figure S 3. a) original TEM image; b) image after adjusting brightness and contrast, removing background noise and applying "despeckle" and "remove outliers" filters; c) binary image with "watershed" filter applied; d) shape profile actually measured by the software.

Among all the parameters measured by the software, two are of interest: Feret diameter and circularity. Feret diameter is the longest distance between any two points of the boundary selected for the measurement. This descriptor tends to overestimate the particle's size, but since particles' projections are almost circular (C~0.9), it can be approximated to the actual size. Circularity is a shape descriptor which measures the "roundness" of a bidimensional shape (*i.e.,* its similarity to a circle), and is calculated with the formula:

$$C = 4\pi \cdot \frac{A}{P^2} \tag{S3}$$

where A and P are area and perimeter of measured particles. C values can be associated with different shapes: for a perfect circle with a smooth surface $C = 1$, while for other shapes the parameter decreases[12].

The data obtained from the elaboration are used to compute the frequency counts over size and circularity values. All the distributions can be fitted with a Log-Normal distribution:

$$P = \frac{f}{\sigma d\sqrt{2\pi}} \cdot e^{-\frac{\left(\ln \frac{d}{\langle d \rangle}\right)^2}{2\sigma^2}} \tag{S4}$$

where f is a prefactor, σ is the standard deviation and $\langle d \rangle$ is the median value of the diameters d. To define the values' polydispersion it is possible to define the empirical parameter PD using the median $\langle d \rangle$ as the average d:

$$PD = 100 \cdot \frac{\sigma}{\langle d \rangle} \tag{S5}$$

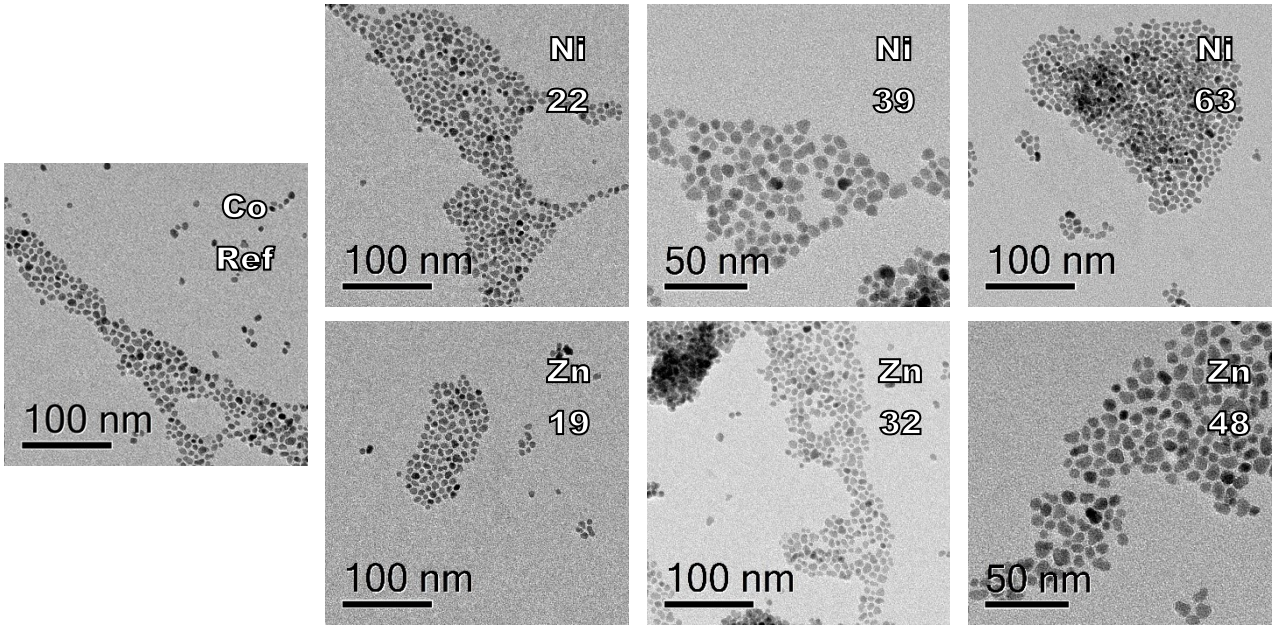

Figure S 4: TEM pictures for each sample

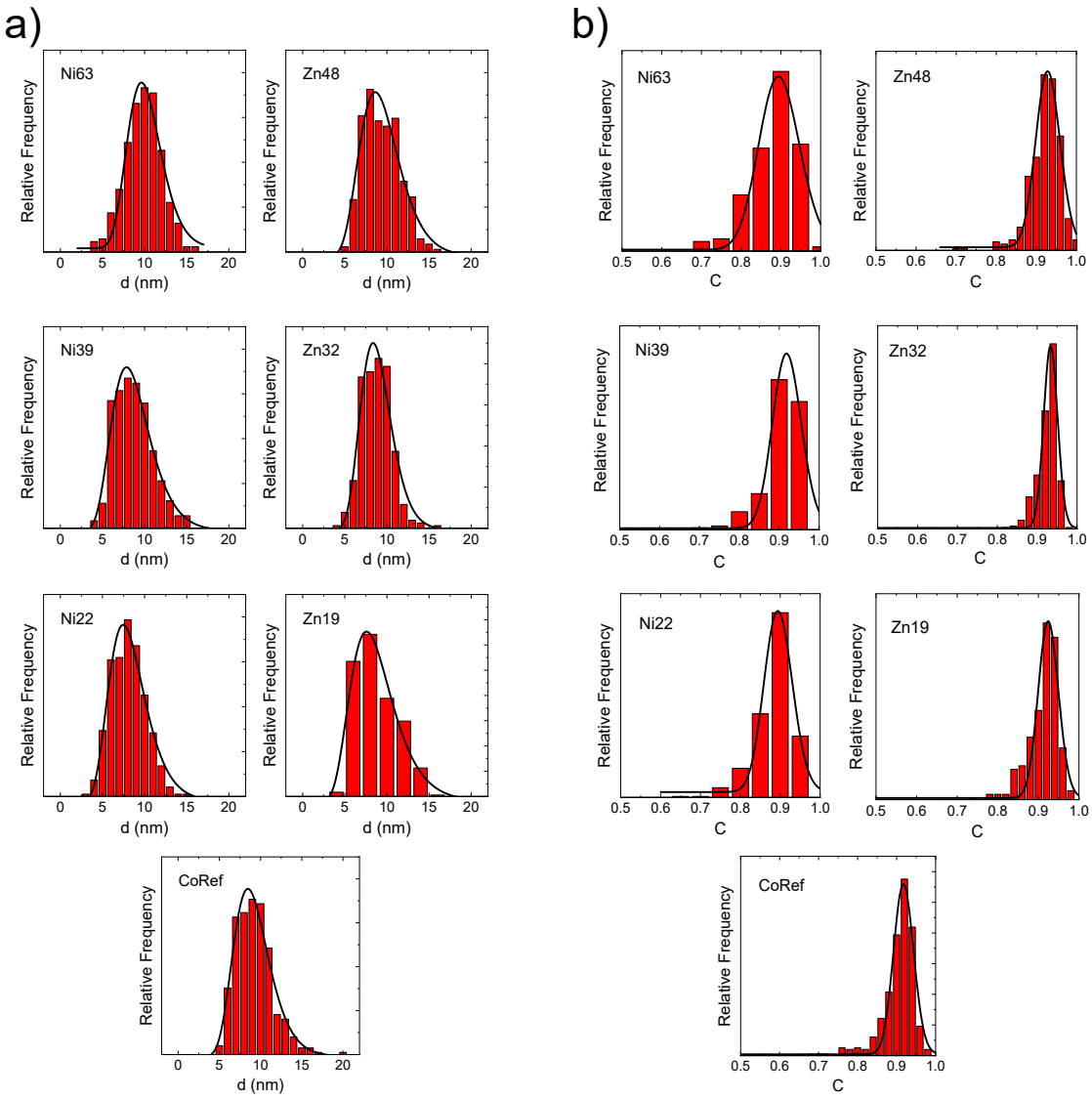

Figure S 5: a) size distributions and b) circularity distributions extracted from the TEM images.

Table S 1: the stoichiometry expected from the synthesis next to the experimental one; the last columns show samples' circularity and polydispersity from TEM measurements.

Sample	**Expected from synthesis**	**Experimental formula (ICP)**	***C***	***PD*** (nm^{-1})
CoRef	$CoFe_2O_4$	$Co_{0.85}Fe_{2.15}O_4$	0.92(1)	2.8(1)
Zn19	$Zn_{0.25}Co_{0.75}Fe_2O_4$	$Zn_{0.19}Co_{0.70}Fe_{2.11}O_4$	0.93(1)	3.9(1)
Zn32	$Zn_{0.50}Co_{0.50}Fe_2O_4$	$Zn_{0.32}Co_{0.47}Fe_{2.22}O_4$	0.93(1)	2.4(1)
Zn48	$Zn_{0.75}Co_{0.25}Fe_2O_4$	$Zn_{0.48}Co_{0.26}Fe_{2.26}O_4$	0.93(1)	2.9(1)
Ni22	$Ni_{0.25}Co_{0.75}Fe_2O_4$	$Ni_{0.22}Co_{0.71}Fe_{2.07}O_4$	0.89(1)	3.5(1)
Ni39	$Ni_{0.50}Co_{0.50}Fe_2O_4$	$Ni_{0.39}Co_{0.45}Fe_{2.16}O_4$	0.92(1)	3.3(1)
Ni63	$Ni_{0.75}Co_{0.25}Fe_2O_4$	$Ni_{0.63}Co_{0.23}Fe_{2.14}O_4$	0.90(1)	2.1(1)

S4. Thermogravimetric analysis

Thermo-Gravimetric Analysis (**TGA**) was used to know the amount of organic surfactant coating the NPs' surface; since the magnetization of matter is proportional to its mass, knowing the amount of diamagnetic organic coating is necessary to normalize magnetization data. Further, quantifying ligand shell mass is useful to know if the washing procedure was performed correctly, and the mass on the particles' surface corresponds to a single layer of OLAC and OLAM (up to ~ 20%)[10]. The analysis was performed by using a LabsysEvo 1600 DTA/TGA (Setaram); few mg of powders was put in an alumina crucible and heated from 30 to 1000 °C at 10 °C/min under O_2 atmosphere (20 mL/min).

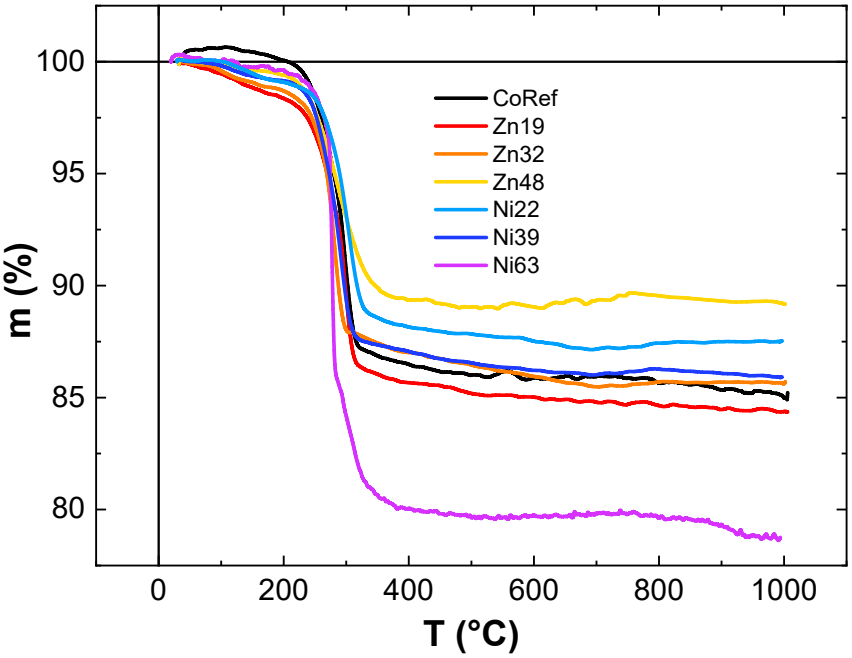

Figure S 6: TGA curves for each sample

S5. Composition

To know the NPs composition, ***Inductively Coupled Plasma – Atomic Emission Spectroscopy*** (**ICP-AES**) was used. Samples were prepared putting 100 µL of NPs solution in 5 mL of HNO_3 (69% w/w%) and heated in a flask on a heating plate at 100 °C until the red nitrogen oxides fumes disappeared. The solutions were then diluted to 50 mL with deionized water and given to the instrument. ICP analyses were entrusted to the Analytical Chemistry Group at the Dipartimento di Chimica e Chimica Industriale (UNIGE) and performed with an iCAP 6300 DUP ICP-AES spectrometer (ThermoScientific). The samples were prepared putting 100 µL of solution in 5 mL of HNO_3 (69% w/w%) and heated in a flask on a heating plate at 100° C until the red nitrogen oxides fumes disappeared. The solutions were then diluted to 50 mL with deionized water and given to the instrument. Respect to the precursor ratios used to synthesize our materials, a lower amount of M^{2+} cations is experimentally observed; this can be attributed to different reaction kinetics, different stabilities[13] or different solubilities of the metallic complexes formed during the synthesis.

S6. ZFC/FC magnetization

Table S 2: TEM and XRPD NPs diameters, T_b and T_{max} calculated for each sample.

Sample	$\langle d \rangle_{XRD}$ (nm)	$\langle d \rangle_{TEM}$ (nm)	T_b (K)	T_{max} (K)	T_{irr} **(3%)** (K)
CoRef	8.3(4)	9.0(1)	199	289	318
Ni22	8.0(4)	8.1(1)	166	252	288
Ni39	8.3(5)	8.5(1)	166	228	328
Ni63	8.3(5)	10.0(1)	107	157	174
Zn19	9.3(4)	8.4(2)	207	285	299
Zn32	9(1)	8.7(1)	166	228	244
Zn48	8.6(5)	9.3(2)	132	201	206

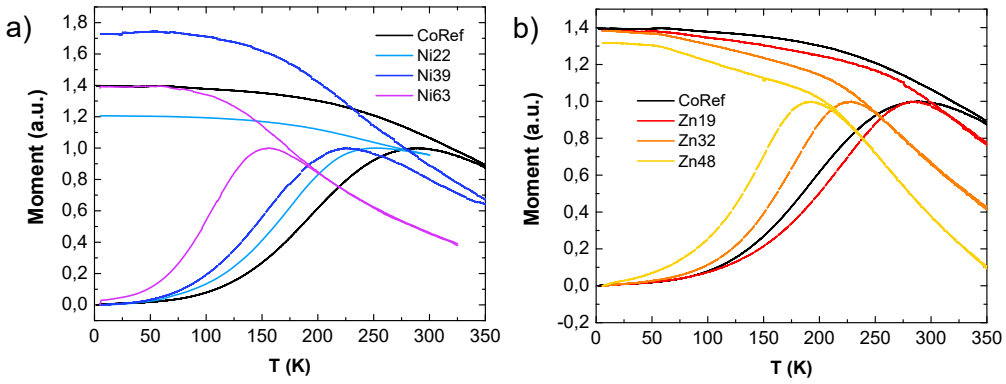

Figure S 7: ZFC/FC curves for a) Ni- and b) Zn-series, normalized for the T_{max} magnetization value.

S7. Néel two sublattice model

Considering that net magnetic moment of spinel ferrite is superposition of magnetic moments of cations in Oh and Td sites which are antiferromagnetically oriented:

$$\mu_{tot} = \sum \mu_{Oh} - \sum \mu_{Td}. \quad \text{(S6)}$$

the M_s values can be estimated by the Néel two sublattice model, considering the well-known ion site selectivity of Ni^{2+} for Oh-sites[14] and of Zn^{2+} for Td-sites[15]) and the spin-only magnetic moment of our metal cations (Zn^{2+} = 0 μ_B, Co^{2+} = 3 μ_B, Ni^{2+} = 2 μ_B, Fe^{3+} = 5 μ_B)[16]. For both series, an equation was written to express the M_s as a function of the stoichiometric coefficient of M^{2+} (x) and the one of Co^{2+} in Oh-sites (y, corresponding to δ) considering following sublattice structure:

$$CoFe_2O_4 \rightarrow [Co_{1-y}Fe_y]_{Td}[Co_yFe_{2-y}]_{Oh}; \quad \text{(S7)}$$

$Ni_xCo_{1-x}Fe_2O_4 \rightarrow [Co_{1-x-y}Fe_{y+x}]_{Td}[Co_yFe_{2-x-y}Ni_x]_{Oh}$;

$Zn_xCo_{1-x}Fe_2O_4 \rightarrow [Co_{1-x-y}Fe_yZn_x]_{Td}[Co_yFe_{2-y}]_{Oh}$;

For Ni-series $Ni_xCo_{1-x}Fe_2O_4$, the Bohr magneton magnetization can be found as follows

$$\mu_{fu}^{Ni}(x;y) = [\mu^{Fe}\cdot(2-x-y) + \mu^{Co}\cdot y + \mu^{Ni}\cdot x] - [\mu^{Fe}\cdot(x+y) + \mu^{Co}\cdot(1-x == 7-5x-4y \quad \text{(S8)}$$

While for the Zn-series $Zn_xCo_{1-x}Fe_2O_4$, the expression is:

$$\mu_{fu}^{Zn}(x;y) = [\mu^{Fe}\cdot(2-y) + \mu^{Co}\cdot y] - [\mu^{Fe}\cdot y + \mu^{Co}\cdot(1-x-y)] = [5\cdot(2-y) \quad \text{(S9)}$$

S8. Mössbauer spectrometry

Mössbauer spectra, obtained at 12 K under an applied field of 8 T, were measured on two representative samples, hereafter named Zn38 and Ni31. The cationic distribution data were used to calculate the magnetic saturation of the two samples and compare the result with the 5 K trend of the two series according to the model and the assumptions described in the main text. Information regarding the cationic distribution of iron were used to assign the distribution of Co^{2+}, and then access to y value and place a dot on the $M_s(x,y)$ map.

Table S 4: Mössbauer parameters extracted from the fitting: the isomer shift (δ), the quadrupole shift (2ε), the effective field (B_{eff}), the hyperfine field (B_{hyp}), the average canting angle (θ) and the ratio of each Fe ion.

Sample	**Site**	$\langle\delta\rangle$ (mms^{-1})	$\langle 2\varepsilon\rangle$ (mms^{-1})	$\langle B_{eff}\rangle$ (T)	$\langle B_{hyp}\rangle$ (T)	$\langle\theta\rangle$ (°)	$\mathbf{Fe_{Td,Oh}^{3+}}$ / $\mathbf{Fe_{total}^{3+}}$
Zn38	**Td**	0.33	-0.02	60.1	52.7	21	32
	Oh	0.48	-0.05	45.4	53.1	18	68
Ni31	**Td**	0.35	0.06	59.7	52.1	18	41
	Oh	0.50	-0.05	46.5	54.2	17	59

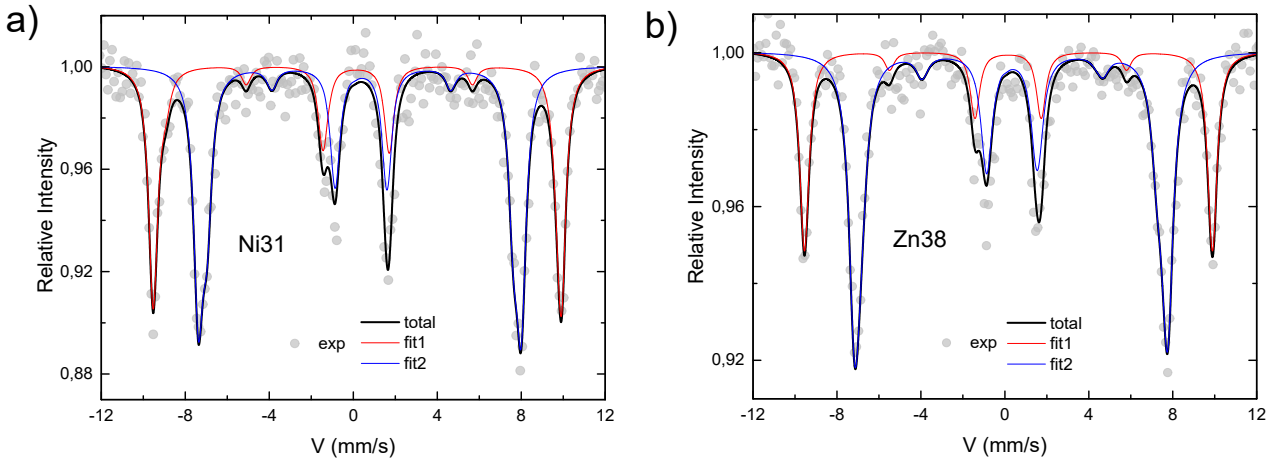

Figure S 8: Mössbauer spectra of a) Zn38 and b) Ni31, obtained at 12 K under external applied field o 8 T..

Bibliography

1 G. Muscas, N. Yaacoub, G. Concas, F. Sayed, R. Sayed Hassan, J. M. Greneche, C. Cannas, A. Musinu, V. Foglietti, S. Casciardi, C. Sangregorio and D. Peddis, Evolution of the magnetic structure with chemical composition in spinel iron oxide nanoparticles, *Nanoscale*, 2015, **7**, 13576–13585.

2 U. B. Sontu, N. G. Rao, F. C. Chou and V. M. Ramana Reddy, Temperature dependent and applied field strength dependent magnetic study of cobalt nickel ferrite nano particles: Synthesized by an environmentally benign method, *J. Magn. Magn. Mater.*, 2018, **452**, 398–406.

3 N. B. Velhal, N. D. Patil, A. R. Shelke, N. G. Deshpande and V. R. Puri, Structural, dielectric and magnetic properties of nickel substituted cobalt ferrite nanoparticles: Effect of nickel concentration, *AIP Adv.*, 2015, **5**, 097166.

4 M. Albino, E. Fantechi, C. Innocenti, A. López-Ortega, V. Bonanni, G. Campo, F. Pineider, M. Gurioli, P. Arosio, T. Orlando, G. Bertoni, C. De Julián Fernández, A. Lascialfari and C. Sangregorio, Role of Zn^{2+} Substitution on the Magnetic, Hyperthermic, and Relaxometric Properties of Cobalt Ferrite Nanoparticles, *J. Phys. Chem. C*, 2019, **123**, 6148–6157.

5 V. Mameli, A. Musinu, A. Ardu, G. Ennas, D. Peddis, D. Niznansky, C. Sangregorio, C. Innocenti, N. T. K. Thanh and C. Cannas, Studying the effect of Zn-substitution on the magnetic and hyperthermic properties of cobalt ferrite nanoparticles, *Nanoscale*, 2016, **8**, 10124–10137.

6 G. Muscas, S. Jovanović, M. Vukomanović, M. Spreitzer and D. Peddis, Zn-doped cobalt ferrite: Tuning the interactions by chemical composition, *J. Alloys Compd.*, 2019, **796**, 203–209.

7 R. Topkaya, A. Baykal and A. Demir, Yafet–Kittel-type magnetic order in Zn-substituted cobalt ferrite nanoparticles with uniaxial anisotropy, *J. Nanoparticle Res.*, 2013, **15**, 1359.

8 G. Barrera, M. Coisson, F. Celegato, S. Raghuvanshi, F. Mazaleyrat, S. N. N. Kane and P. Tiberto, Cation distribution effect on static and dynamic magnetic properties of $Co_{1-x}Zn_xFe_2O_4$ ferrite powders, *J. Magn. Magn. Mater.*, 2018, **456**, 372–380.

9 D. D. Andhare, S. R. Patade, J. S. Kounsalye and K. M. Jadhav, Effect of Zn doping on structural, magnetic and optical properties of cobalt ferrite nanoparticles synthesized via. Co-precipitation method, *Phys. B Condens. Matter*, 2020, **583**, 412051.

10 D. Peddis, F. Orrù, A. Ardu, C. Cannas, A. Musinu and G. Piccaluga, Interparticle Interactions and Magnetic Anisotropy in Cobalt Ferrite Nanoparticles: Influence of Molecular Coating, *Chem. Mater.*, 2012, **24**, 1062–1071.

11 V. K. Pecharsky and P. Y. Zavalij, *Fundamentals of Powder DIffraction and Structural Characterization of Materials*, Springer, 2008.

12 G. Muscas, G. Singh, W. R. Glomm, R. Mathieu, P. A. Kumar, G. Concas, E. Agostinelli and D. Peddis, Tuning the size and shape of oxide nanoparticles by controlling oxygen content in the reaction environment: Morphological analysis by aspect maps, *Chem. Mater.*, 2015, **27**, 1982–1990.

13 S. Gyergyek, D. Makovec, A. Kodre, I. Arčon, M. Jagodič and M. Drofenik, Influence of synthesis method on structural and magnetic properties of cobalt ferrite nanoparticles, *J. Nanoparticle Res.*, 2010, **12**, 1263–1273.

14 C. Yang, Y. Hu, X. Li, J. Li, L. Wang and H. Li, Tuning of magnetic properties and hyperfine interaction by the substitution of Ni^{2+} for cobalt ferrite nanoparticles, *J. Mater. Sci. Mater. Electron.*, 2019, **30**, 19647–19653.

15 H. L. Andersen, C. Granados-Miralles, M. Saura-Múzquiz, M. Stingaciu, J. Larsen, F. Søndergaard-Pedersen, J. V. Ahlburg, L. Keller, C. Frandsen and M. Christensen, Enhanced intrinsic saturation magnetization of $Zn_xCo_{1-x}Fe_2O_4$ nanocrystallites with metastable spinel inversion, *Mater. Chem. Front.*, 2019, **3**, 668–679.

16 B. D. Cullity and C. D. Graham, *Introduction to Magnetic Materials*, John Wiley & Sons, Inc., Hoboken, NJ, USA, 2008.